Decellularized Dermis Extracellular Matrix Alloderm as a Scaffold for Biological Engineered Blood Vessels

Bijal Patel
Wayne State University
Dan Saliganan
Wayne State University
Ali Rteil
Henry Ford Health System
Loay Kabbani
Henry Ford Health System
Mai Lam (mtlam@wayne.edu)
Wayne State University

Research Article

Keywords: vascular graft, human-derived materials, biological engineered blood vessels (BEBVs), encourage extracellular matrix (ECM)

Posted Date: December 29th, 2020

DOI: https://doi.org/10.21203/rs.3.rs-133012/v1

Abstract

The ideal engineered vascular graft would utilize human-derived materials to minimize foreign body response and tissue rejection. Current biological engineered blood vessels (BEBVs) inherently lack the structure required for implantation. Current methods of mechanical conditioning to encourage extracellular matrix (ECM) deposition requires weeks to months, impeding translation. We hypothesized that an ECM scaffold would provide the structure needed. Skin dermis ECM is commonly used in reconstructive surgeries, is commercially available and is FDA-approved. We evaluated the commercially available decellularized skin dermis ECM called Alloderm for its efficacy in providing structure to biological engineered blood vessels. Alloderm was seeded with fibroblast cells typically found in the adventitia during integration into our lab's unique protocol for generating BEBVs. To assess structure, tissue mechanics were analyzed. Standard BEBVs without Alloderm exhibited a tensile strength of 67.9 ± 9.78 kPa, whereas Alloderm integrated BEBVs showed a significant increase in strength to 1500 ± 334 kPa. In comparison, native vessel strength is 1430 ± 604 kPa. Burst pressure reached 51.3 ± 2.19 mmHg. Total collagen and fiber maturity were significantly increased due to the presence of the scaffolding material. These results demonstrate the success of Alloderm to provide structure to BEBVs in an effective way.

Introduction

Current technologies in vascular tissue engineering rely on polymer tubes as a scaffolding material or cell sheets wrapped into a tube. Leading approaches share the same basic principles- seeding of vascular smooth muscle cells onto a tubular scaffold such as a polymer[1–3] or hydrogel[4–6], followed by weeks of mechanical conditioning for extracellular matrix deposition to increase vessel strength, and finally decellularization to remove immunogenic components. However, polymers can lead to graft failure due to the body's natural foreign body response leading to a persistent inflammatory response[7]. The hydrogel grafts are completely biological and thus illicit minimal immune response, however presently the most effective current way to achieve sufficient strength is to subject these vessels to mechanical conditioning for several weeks to months, which has impeded manufacturability and translatability. Another common approach to engineer blood vessels is to roll cell sheets into tubes creating a completely biological construct[7–8]. However, this approach still requires weeks of strength conditioning. A more efficient approach for introducing the strength needed for implantation.

We hypothesized that using a human-derived, biological material as scaffolding as opposed to polymers commonly used in the field will provide an effective support structure that will meet the mechanical needs of a vascular graft and minimize adverse immune response. In a native blood vessel, the adventitia outer layer is key to providing structural integrity[9–11]. The extracellular matrix of the adventitia allows for a vessel to withstand high pressures preventing vessel rupture[12]. The strength derives from the significant type I collagen content, which is a load bearing extracellular matrix protein that is able to resist high pressure forces[13–16]. The adventitia also contains elastin to aid in elasticity and vessel distension[17].

Collagen is found in many organs, with especially high levels in the skin. Specifically, the ECM of the skin dermis consists of type I collagen and elastin to aid in strength and elasticity[18], thus providing an ECM similar to that of the adventitia. Decellularized dermis ECM has been used for years in reconstructive surgeries and for wound care, with several products currently on the market[19]. One product in particular, Alloderm, has been used extensively in the clinic with much success. Alloderm is a human allograft, and has been used for reconstructive surgeries, complex abdominal wall hernia repair, soft-tissue defect augmentation, rhinoplasty, and vaginal repair[18–22]. Alloderm has also been investigated for other uses such as for tendon repair, stress urinary incontinence and pelvic organ prolapse repair[23–24]. The mechanical properties of the ECM of Alloderm, and the fact that it is decellularized thus reducing inflammatory and rejection risk, makes it ideal for tissue engineering application[20,25–27]. Thus, we proposed to employ the advantageous properties of Alloderm to mimic the adventitia's role and provide strength to engineered blood vessels. This type of application of a decellularized matrix is a departure from the typical use of decellularized matrices as a scaffold for use in its tissue of origin. Our approach represents an innovative application of a decellularized ECM for use as a reinforcement material in an engineered tissue of a different tissue origin. Our objective was to mimic the natural strength component of a native blood vessel by substituting a comparable ECM.

Using our lab's unique method for generating completely biological engineered blood vessels (BEBVs) as our base structure[28–30]. Alloderm was integrated into our protocol. In our methods, vascular cells are formed into ring structures, which are then stacked into tubular form to form the vessel. This method is termed the Ring Stacking Method (RSM). This method is highly modifiable and allows for the integration of reinforcing materials such as Alloderm. Once the Alloderm material was successfully added to our RSM protocol, the resultant engineered rings and vessel structures were tested mechanically. Tensile tests revealed that the Alloderm-integrated engineered vessels reached a tensile strength of 1500 ± 334 kPa, which is within range of a native vessel's tensile strength of 1430 ± 604 kPa[12]. Burst pressure reached 80 mmHg, indicating that the decellularized ECM was able to increase the completely biological engineered vessels blood pressure capabilities to within the diastolic blood pressure range. Histological analysis showed that the overall collagen amount and degree of fiber maturity were significantly increased, elements that both contribute to tissue strength. These results demonstrate the success of Alloderm to provide sufficient support to the BEBVs in a much more efficient and effective way than current approaches in the field.

Methods

Cell culture.

Human dermal fibroblasts (HuDF) (PCS-201-012, ATCC, Manassas, VA) were used to make the engineered vessels. Fibroblasts were chosen to coincide with the adventitia-based protocol presented here. Dermal fibroblasts were chosen in foresight of patient application of autologous cells. Passages up to 15 were able to form consistent rings/vessels. Fibroblast growth media (GM) consisting of 89% Dulbecco's

Modified Eagle Medium (DMEM), 10% fetal bovine serum, and 1% antibiotic/antimycotic was used to expand and maintain the cell culture. Cells were trypsinized at roughly 90% confluency and used to make the rings and vessel structures.

Human saphenous veins.

Human saphenous veins were obtained from diabetic patients undergoing limb amputation between years 2018–2020. The study was approved by the Human Institutional Review Boards of both entities of Wayne State University and Henry Ford Health System (IRBs 054514M1E and 10744, respectively). Informed consent was obtained from all 6 patients who donated tissues. The tissues were obtained in accordance with relevant guidelines and regulations.

Assembly of ring formation plates.

A 60 mm petri dish was used as the basis for forming the rings. Poly(dimethylsiloxane) (PDMS) polymer (1064291, Dow Corning, Midland, MI) was used to coat plates at 3 mL per plate. Posts were made and adhered to the plates centrally to provide a structure around which the rings would form. The posts were punched from PDMS bulk material using 6 mm diameter biopsy punches to fabricate 6 mm lumen vessels. Base plates were coated with PDMS, followed by placement of the post centrally in the plate and oven cured at 60 °C for 1 h. Plates were sterilized with a 30 minute 70% ethanol soak followed by 30 minutes of UV sterilization under the bio-hood.

Hydrogel formulation.

A provisional hydrogel was used to secure the cell sheet as it aggregated around the central post to form the ring structures. Hydrogels rapidly degrade in 2–4 weeks hence serving as a temporary support. Fibrin gel was identified as an ideal option as it is naturally found in the body. Fibrin hydrogels were formed using thrombin, fibrinogen, and hydrogel media[28]. A 4:1 ratio of 20 mg/mL bovine fibrinogen (151122, MP Biomedicals LLC, OH) to 100 U/mL bovine plasma thrombin (7592, BioVision, Milpitas, CA) was prepared. Hydrogel media consisted of 88.8% DMEM, 0.1% TGF-β and ascorbic acid, 10% fetal bovine serum, and 1% antibiotic/antimycotic.

Alloderm preparation.

Alloderm was obtained from LifeCell Corporation (Allergan, CA). Biopsy punches were used to cut 6 mm holes into Alloderm. A scalpel was used to cut a 3-3.5 mm width around the 6 mm hole. The final dimensions of the donut shaped Alloderm was an inner diameter of 6 mm and outer diameter around 12–13 mm. Alloderm donuts were sterilized in a bio-hood using UV sterilization for 15 minutes on both sides and kept sterile until ready to use.

Ring formation.

Cultured fibroblasts were trypsinized from pates and re-suspended in growth media. Each prepared PDMS ring plate was seeded with 1.5×10^6 fibroblast cells in 4 mL GM, 150 µg ascorbic acid and 0.01 ng TGF-β either onto fibrin gel directly (basic rings/vessels) or fibrin gel topped with Alloderm (ECM-integrated rings/vessels). Media was changed one day after seeding, and subsequently every 3 days for 14 days. Each media change was supplemented with fresh ascorbic acid and TGF-β.

Fabrication of dermis-integrated engineered vessels.

To create the vascular grafts, tubular structures were created by stacking 3 or more engineered rings. Alloderm adventitia vessels were created using our lab's Ring Stacking Method (RSM). In the RSM, engineered vascular rings are stacked around a 1.2 cm long 3D printed post placed centrally in custom made 8 cm tall plates. Engineered vessels made of stacks of 3 rings were used for histology and stacks of 6 rings were used for mechanical testing. Rings were temporarily adhered to one another using additional fibrin glue to secure the rings to each other as the cells deposited their own extracellular matrix to secure the overall vascular structure. A 1:1 volumetric ratio of 30 µL of 100 u/mL thrombin to 30 µL of 20 mg/mL fibrinogen was used for the fibrin glue. Ring stacks, i.e. vessels, were maintained in HuDF growth media supplemented with ascorbic acid and TGF-β for one week with a media change 3 days after stacking.

Mechanical testing.

Tensile testing was performed using an UStretch system with a 5 N load cell (CellScale, Waterloo, Ontario, Canada) and an Instron 5943 with a 50 N and a 500 N load cell (Instron, Norwood, MA). The smaller load UStretch was used for tensile testing in the range of the original rings and vessels without Alloderm. The higher load Instron was used to tensile test the Alloderm by itself, and Alloderm-integrated rings and vessels. Rings were tensile tested 14 days after cell seeding. Two modes of tensile testing were conducted to analyze both circumferential and longitudinal vessel mechanics. Circumferential tensile testing was used to measure the hoop strength of the rings and vessels. Longitudinal testing was used to measure the strength along the length of the vessels. Samples were stretched to failure and mechanical properties of elastic modulus, ultimate tensile strength and failure strength were obtained from resultant stress-strain curves.

Circumferential tensile testing was conducted at a strain rate of 0.4 mm/min until failure. Rings with Alloderm (n = 5) and without dermis (n = 5) were tested to determine the effect of the addition of Alloderm. Alloderm donuts alone (n = 6) were tensile tested to determine their independent mechanical properties. For tensile testing, engineered vessels were built with 6 rings each. Vessels with (n = 5) and without (n = 5) Alloderm were tensile tested after a 7-day culture period following ring stacking. For

control data, human native vessels were obtained (n = 6) and tensile tested. Human saphenous veins from diabetic patients following amputation.

Longitudinal tensile testing was performed at a strain rate of 0.4 mm/min until failure. Engineered vessels with (n = 5) and without Alloderm (n = 5) were tensile tested following a 7 day culture period after ring stacking. In order to attach the vessels longitudinally into the tensile tester, VetBond tissue adhesive (3 M, St. Paul, MN) was used to fix the two ends of the vessels onto sandpaper, which was then folded and placed on the Ustretch system hooks.

Histology.

Engineered rings and vessels were histologically analyzed to determine tissue structure; and ECM content and organization. Tissues were processed in paraffin. Individual rings and 3-ring vessels with and without Alloderm were fixed in formalin for 48 hours. Samples were stored in 70% ethanol in 5ºC until dehydrated. Samples were dehydrated in graduations of 70–100% ethanol over 12 hours and then embedded into paraffin blocks. Hematoxylin and eosin (H&E), Masson's Trichrome, and Picrosirius red stains were conducted on all ring groups and Alloderm donuts. H&E revealed cellular and extracellular matrix organization. DAPI stain was used to determine cellularity. Masson's Trichrome and Picrosirius red stains showed collagen organization and total content in the rings and Alloderm donuts. Collagen quantification for red and blue stained collagen from picrosirius red and trichome, respectively, were quantified as a percentage of total cross-sectional area using ImageJ.

Polarized light.

Picrosirius red stained samples of rings and Alloderm donuts were observed under polarized light to determine collagen maturity of each sample. Birefringence images were captured using an Axiovert 200 microscope (Carl Zeiss, Oberkochen, Germany). Mature, thicker collagen fibers appear orange and red under polarized light. Immature, thinner collagen fibers appear yellow and green under polarized light. Polarized light images were quantified for percent cross-sectional area of red, yellow and green fibers using ImageJ.

Hemodynamic testing.

The hemodynamic capabilities of the engineered vessels were assessed by burst pressure testing. Burst pressure gives an indication of the maximum pressure the ECM-integrated BEBVs can withstand. Alloderm-integrated vessels were subjected to pulsatile flow with cell culture media in a custom-made bioreactor with a peristaltic pump (WT600-2J, Longer Precision Pump Cp. Ltd, Boonton, NJ), a glass media reservoir, polymer tubing, a custom-made bioreactor chamber, and 3D printed vessel holders.

Vessels were secured onto 3D printed vessel holders using VetBond. Alloderm vessels (n = 5) were subjected to increasing fluid pressure until failure.

Suture retention.

Suture retention tests were conducted to examine the graft's ability to mechanically retain a suture placed using standard surgical technique. These tests were conducted using the UStretch system. Engineered vessels with (n = 5) and without Alloderm (n = 5) were tested following a 7 day culture period after ring stacking. Sutures sized 6 – 0 proline were sutured through the bottom end of the vessel and then fixed to the bottom hook of the UStretch system using sandpaper and gorilla glue. The top stationary hook on the Ustretch system held the engineered vessels fixed in place using VetBond and sandpaper. The suture was pulled at a strain rate of 0.4 mm/min until the failure. Force output during the duration of the test was recorded and plotted versus displacement.

Statistics.

Statistical analyses were conducted using SPSS (IBM, Armonk, New York). Results were presented as means with standard error of means. One-way ANOVA were performed to compare material properties determined from circumferential tensile testing of rings and vessels. Tukey B post-hoc test was used to determine significance between groups. Student's t-test was performed to compare engineered vessels with and without Alloderm for longitudinal tensile testing, suture retention and burst pressure comparisons. The alpha level was set to 0.05.

Results

Ring and vessel formation.

The Alloderm decellularized dermis was incorporated into our tissue engineered vessel protocol[28–30] as depicted in Fig. 1. The Alloderm material exhibited some additional stiffness compared to fresh dermis tissue determined by observation, likely due to the proprietary treatment protocol for commercialization[31]. The human dermal fibroblasts were able to infiltrate the Alloderm material once seeded. Alloderm did not hinder ring formation and integrated into the lumen side of the ring structures and vessels.

Ring mechanics.

Circumferential ring tensile mechanics significantly improved with inclusion of Alloderm in the rings and vessels. Average stress-strain curves for rings without Alloderm, rings with Alloderm and Alloderm donuts are shown in Fig. 2 and material properties are summarized in Table 1. Average elastic modulus, ultimate tensile strength and failure strength for rings without Alloderm (n = 5) were 89.1 ± 27.5 kPa, 177 ±

21.4 kPa and 101 ± 34.8 kPa, respectively. Rings with Alloderm (n = 5) had an elastic modulus of 6630 ± 1510 kPa and an ultimate tensile strength of 1770 ± 221 kPa. Alloderm rings exhibited two main rupture points, consisting of the Alloderm completely tearing first at 1500 ± 372 kPa, followed by the remaining cells and hydrogel structure tearing to failure at 6.75 ± 3.25 kPa (Supplemental Video 1). Average elastic modulus, ultimate tensile strength and failure strength for Alloderm donuts alone (n = 4) were 8250 ± 3360 kPa, 4730 ± 628 kPa and 4390 ± 848 kPa, respectively. The percent elongation of rings, Alloderm rings and Alloderm donuts was 310 ± 29.8%, 162 ± 48.3% and 89.9 ± 16.3%, respectively.

Table 1
Average Circumferential Ring Mechanical Properties

Group	E (kPa)	UTS (kPa)	FS Primary (kPa)	FS Secondary (kPa)	Percent Elongation (%)
Standard Rings (n = 5)	89.1 ± 27.5[a,c]	177 ± 21.4[a,c]	101 ± 34.8[a,c]	N/A	310. ± 29.8[a,c]
Alloderm Rings (n = 5)	6628 ± 1506[a]	1765 ± 221[b,a]	1498 ± 372[b,a]	6.75 ± 3.25	162 ± 48.3[b,a]
Alloderm Alone (n = 4)	8254 ± 3358[c]	4731 ± 848[b,c]	4388 ± 848[b,c]	N/A	89.9 ± 16.3[b,c]
[a] Statistically significant difference between standard rings and Alloderm rings (E: $p \leq 0.0010$; UTS: $p < 0.0001$; FS Primary: $p < 0.01$; Percent Elongation: $p < 0.001$)					
[b] Statistically significant difference between Alloderm rings and Alloderm alone (E: not significant; UTS: $p < 0.0001$; FS Primary: $p < 0.0001$; Percent Elongation: $p < 0.05$)					
[c] Statistically significant difference between standard rings and Alloderm alone (E: $p < 0.0001$; UTS: $p < 0.0001$; FS Primary: $p < 0.0001$; Percent Elongation: $p < 0.001$)					

Vessel mechanics.

Engineered vessel tensile mechanics significantly improved with inclusion of Alloderm. Average stress-strain curves for rings without Alloderm, rings with Alloderm and Alloderm donuts are shown in Fig. 3a-e and summarized in Table 2. Interestingly, initial (FS1) and complete (FS2) failure points were noted for the vessel groups, indicating the point of failure of the first and last ring, respectively. These two failure points are of importance to note because the initial point of failure is vital information for clinical application, as is the catastrophic point of complete vessel failure. Average elastic modulus and ultimate tensile strength for vessels without Alloderm (n = 5) were 79.4 ± 11.6 kPa and 67.9 ± 9.78 kPa, respectively. The primary failure point and secondary failure point of standard rings were 49.8 ± 27.1 kPa and 3.22 ± 1.47 kPa, respectively. Average elastic modulus and ultimate tensile strength for Alloderm vessels (n = 5) were 3720 ± 686 kPa and 1500 ± 334 kPa, respectively. The primary failure point and

secondary failure point for Alloderm vessels were 1397 ± 301 kPa and 4.77 ± 1.73 kPa, respectively (Supplemental Video 2). To compare the contribution of the Alloderm material alone in the vessels, 6 Alloderm donuts were adhered with Vetbond and tensile tested. Average elastic modulus and ultimate tensile strength of the 6 Alloderm donuts (n = 4) were 11.3 ± 1.96 MPa and 5049 ± 333 kPa, respectively. The primary failure point and secondary failure point were 4790 ± 348 kPa and 119 ± 39.2 kPa, respectively. Percent elongation for vessels without Alloderm, Alloderm vessels and 6 Alloderm donuts alone were 511 ± 65.0%, 286 ± 56.1% and 105 ± 12.3%, respectively. To evaluate the Alloderm vessels compared to native vessels, human saphenous vein was also mechanically tested. Interestingly, the Alloderm vessels surpassed circumferential tensile mechanics of native human saphenous vein (n = 5), which exhibited an elastic modulus of 2980 ± 410 kPa, ultimate tensile strength of 1060 ± 155 kPa and failure strength of 416 ± 157 kPa. The native human vessel had an average percent elongation of 120 ± 19.6%.

Table 2
Average Circumferential Vessel Material Properties

Group	E (kPa)	UTS (kPa)	FS1 (kPa)	FS2 (kPa)	Percent Elongation (%)
Standard Vessels (n = 5)	79.4 ± 11.6[a,b,c]	67.9 ± 9.78[a,b,c]	49.8 ± 27.1[a,b]	3.22 ± 1.47[b]	511 ± 64.9[a,b,c]
Alloderm Vessels (n = 5)	3721 ± 687[a,d]	1504 ± 262[a,d,e]	1397 ± 301[a, d,e]	4.77 ± 1.73[d]	286 ± 56.1[a,d,e]
Alloderm Alone (n = 4)	11396 ± 1962[b,d,f]	5049 ± 333[b,d,f]	4795 ± 384[b, d,f]	119 ± 39.2[b,d]	3726 ± 733[b,d]
Human Saphenous Vein (n = 6)	2979 ± 409[c,f]	1059 ± 155[c,e,f]	416 ± 157[e,f]	N/A	821 ± 141[c,e]

[a] Statistically significant difference between Standard Vessels and Alloderm Vessels (E: $p < 0.0001$; UTS force: $p < 0.0001$; FS Primary force: $p < 0.0001$; FS secondary: not significant; Percent Elongation: $p < 0.0001$)

[b] Statistically significant difference between Standard Vessels and Alloderm Alone (E: $p < 0.0001$; UTS force: $p < 0.0001$; FS Primary force: $p < 0.0001$; FS secondary: $p < 0.0001$; Percent Elongation: $p < 0.0001$)

[c] Statistically significant difference between Standard Vessels and Diabetic Human Saphenous Vein (E: $p < 0.001$; UTS force: $p < 0.0001$; FS Primary force: not significant; Percent Elongation: $p < 0.0001$)

[d] Statistically significant difference between Alloderm Vessels and Alloderm Alone (E: $p < 0.0001$; UTS force: $p < 0.0001$; FS Primary force: $p < 0.0001$; FS secondary: $p < 0.0001$; Percent Elongation: $p < 0.0001$)

[e] Statistically significant difference between Alloderm Vessels and Diabetic Human Saphenous Vein (E: not significant; UTS force: $p < 0.05$; FS Primary force: $p < 0.0001$; Percent Elongation: $p < 0.0001$)

[f] Statistically significant difference between Alloderm Alone and Diabetic Human Saphenous Vein (E: $p < 0.0001$; UTS force: $p < 0.0001$; FS Primary force: $p < 0.0001$; Percent Elongation: not significant)

Longitudinal tensile mechanics representing strength along the length of the vessels was not significantly different in vessels without Alloderm compared to vessels with Alloderm (Fig. 3f-g, Table 3). The longitudinal elastic modulus, ultimate tensile strength and failure strength for vessels without Alloderm (n = 4) were 26.1 ± 13.5 kPa, 11.2 ± 6.05 kPa and 1.54 ± 0.304 kPa, respectively. The longitudinal elastic modulus, ultimate tensile strength and failure strength for vessels with Alloderm (n = 3) were 10.7 ± 8.09 kPa, 3.47 ± 1.61 kPa and 1.41 ± 1.08 kPa, respectively.

Table 3
Longitudinal Vessel Material Properties

Group	E (kPa)	UTS (kPa)	FS (kPa)
Standard Vessels (n = 5)	26.1 ± 13.5	11.2 ± 6.05[a]	1.54 ± 0.304
Alloderm Vessels (n = 5)	10.7 ± 8.09	3.47 ± 1.61[a]	1.41 ± 1.08

[a]Statistically significant difference between Standard Vessels and Alloderm Vessels (E: no significance; UTS: $p < 0.05$; FS: not significant)

The force required to strain the engineered rings, engineered vessels and Alloderm alone to failure (Supplemental Fig. 1; Supplemental Tables 1 and 2) provide insight into the resultant mechanics and the effects of the difference in cross-sectional area on strength calculations. Significant differences in forces to obtain circumferential elasticity, tensile strength and failure strength were found between standard rings and Alloderm alone ($p < 0.001$). Standard rings had an average elastic force, ultimate tensile force and failure force of 0.127 ± 0.134 N, 0.273 ± 0.134 N and 0.162 ± 0.104 N, respectively. Alloderm alone had an average elastic force, ultimate tensile force and failure force of 21.9 ± 9.31 N, 12.7 ± 2.94 N and 11.8 ± 3.27 N, respectively. Although significant differences were seen in comparing material properties of Alloderm rings to Alloderm alone, when comparing associated forces no significant differences were found between ultimate tensile strengths ($p = 0.102$), and between Alloderm ring primary failure force and Alloderm alone failure force ($p = 0.793$). This indicates that the larger thickness of the Alloderm rings compared to the Alloderm donuts is responsible for the different in calculation of strength due to the difference in cross-sectional area. Alloderm rings had an average elastic force, ultimate tensile force, primary failure force, and secondary failure force of 56.3 ± 6.58 N, 15.1 ± 0.677 N, 12.7 ± 1.94 N, and 0.0558 ± 0.0207 N, respectively. This indicates structural integrity of Alloderm was not comprised when in the rings, but rather the reduced mechanical properties can be attributed to increased cross-sectional area. Between standard rings and Alloderm rings a significant difference was found between elastic force, ultimate tensile force and primary failure strength force ($p < 0.001$). These force outputs indicate the superior tensile mechanics from inclusion of Alloderm into the rings. Using an independent t-test with equal variances not assumed, a significant difference was found between standard rings failure strength and Alloderm ring secondary failure strength ($p < 0.01$), however, this can also be attributed to increased cross-sectional area. Using an independent t-test with equal variances not assumed, no significant difference was found between the standard ring's failure force and Alloderm ring secondary failure force ($p = 0.084$). This indicates that the cells in the fibrin gel maintain their mechanical properties regardless of the inclusion of Alloderm. All together, these results indicate that Alloderm rings are a composite material comprised with material properties of strength from the Alloderm and ductility from the ring of cells organized in the fibrin gel.

Rings and vessels histological analysis.

Histological analysis of rings provided pertinent information on cellular and ECM protein content and organization in the engineered tissue. Vessel histology showed cellular and ECM organization across the multi-ring structure. Cross-sectional ring samples were stained with multiple stains. Hematoxylin and eosin was used to visualize overall cellular structure by staining nuclei deep purple and cytoplasm and extracellular matrix pink. Masson's Trichrome and Picrosirius red stains were used to visualize ECM content and organization, by staining collagen blue and red, respectively. DAPI stains were used to clearly demarcate cell density and location.

In the standard rings (Fig. 4a-c), fibroblasts self-organized into a band of cells surrounded by a layer of the fibrin gel. In rings with Alloderm (Fig. 4d-f), the organization of the ring from the lumen outward was first the Alloderm, followed by cells, then fibrin gel, and lastly more cells lining the outer diameter. Average ring thickness without and with Alloderm was 0.964 ± 0.170 mm and 2.35 ± 0.198 mm, respectively. Cell nuclei were seen located in the fibrin gel and Alloderm indicating cell migration. In rings with Alloderm, Trichrome stain showed a large blue band at the Alloderm, indicating its significant collagen content. In addition, a thin blue band was seen on the outer diameter suggesting collagen deposition by the cells in the Alloderm rings which was not evident in standard rings. This collagen deposition pattern was confirmed in Picrosirius red stained sections where the red collagen-stained areas were seen co-located with the cells and in parts of the hydrogel. In contrast, little positive collagen stain was seen in the standard rings without Alloderm. The same dense blue and red collagen network is seen in the Trichrome and Picrosirius red stains of Alloderm alone (Fig. 4g-i). Both trichrome and picrosirius red stains of the groups showed Alloderm alone had the highest percentage of area stained positive for collagen followed by Alloderm rings and then standard rings. Trichome stains of standard rings and Alloderm rings showed a significant difference ($p < 0.001$) in quantified collagen, 18.8 ± 4.77% and 65.6 ± 14.9%, respectively. Picrosirius red stains of rings without Alloderm and with Alloderm also showed significant differences ($p < 0.001$) in quantified collagen as 21.7 ± 8.27% and 66.7 ± 11.4%, respectively. Both ring groups additionally showed significant differences ($p < 0.001$) in percent area stained collagen from trichrome, 100. ± 0.00%, and picrosirius red, 100. ± 0.00%, in Alloderm alone.

Longitudinal cross sections of vessels with and without Alloderm stained for H&E (Fig. 4j-k) showed successive rings composed of cells, fibrin gel, and Alloderm for the Alloderm rings. Areas of cellular density were evident by the purple nuclei stains. Standard vessels without Alloderm showed cellular organization as dense pockets of cells, whereas Alloderm vessels show more evenly distributed layers of cells.

DAPI fluorescent stains of cell nuclei in Alloderm rings showed the organization of the cells along the outer diameter of the rings (Fig. 5). In comparison, DAPI stains for Alloderm alone were negative indicating the absence of cells. Lack of positive stained DAPI in Alloderm alone indicates cell infiltration in Alloderm rings is from the ring making process rather than possible nuclear remnants from the original material of the decellularized Alloderm.

Polarized light images of a Picrosirius red stained standard ring, Alloderm ring and Alloderm alone (Fig. 6) allowed for further assessment of collagen organization in the rings. Collagen fiber thickness can be visualized using polarized light microscopy of Picrosirius red stained tissues. More mature, thicker fibers appear orange to red whereas less mature, thinner fibers appear green to yellow. Rings without Alloderm primarily exhibited mature red collagen fibers in the region around the cells surrounded by areas of less mature yellow and orange collagen in the fibrin hydrogel. In the Alloderm alone, polarized light showed a dense red network of mature collagen. In the Alloderm ring, a dense red-orange network of collagen is seen in the Alloderm area, along with a lighter region of red fibers and orange fibers deposited by the cells surrounding the Alloderm. These results clearly show the enhanced collagen content provided by the inclusion of the Alloderm into the engineered tissue. Polarized light quantifications for percent area of fibers shows significant differences ($p < 0.01$) in red fibers for all three groups, in yellow fibers for all three groups, and in green fibers ($p < 0.01$) between standard rings and Alloderm alone and between standard rings and Alloderm rings. Standard rings contained 15.8 ± 7.85, 58.2 ± 13.9 and 19.0 ± 8.77 percent area of red, yellow and green collagen fibers, respectively, which was the highest yellow and green fiber content. Alloderm alone contained 91.3 ± 5.55, 7.49 ± 4.91 and 0.757 ± 0.791 percent area of red, yellow and green collagen fibers, respectively, which contained the highest red fiber composition. Alloderm rings contained 73.7 ± 5.49, 22.9 ± 5.41 and 3.47 ± 1.72 percent area of red, yellow and green collagen fibers, respectively, which contained higher red fiber content than similar green fiber content as Alloderm alone.

Suture retention and burst pressure.

No significant differences were found between vessels with and without Alloderm for suture retention (Fig. 7). Average suture retention for vessels without Alloderm ($n = 3$) was 7.73 ± 2.01 gram-force. Average suture retention for vessels with Alloderm ($n = 3$) was 9.83 ± 2.25 gram-force. In both vessel groups, suture retention failure points occurred in the area between the rings, at about 1 to 2 rings above the suture. However, there was a significant difference between burst pressure between vessels with and without Alloderm, with values of 51.3 ± 2.19 mmHg and 47.0 ± 1.14 mmHg, respectively (Fig. 8).

Discussion

The Alloderm ECM resulted in the ideal material for scaffolding tissue engineered blood vessels. Given the Alloderm's pliability and strength, it easily integrated into the aggregating ring structures while concurrently offering sufficient support and strength for the final tissue. The Alloderm ECM organized into the lumen side of the ring and was lined by the fibrin gel and cells on the outer edge. This organization allowed the Alloderm to serve as the main component to counteract forces exerted on the tissue while the cells on the outer edge provided elasticity. This observation was supported by the tensile results showing two main failure points- first, of the stiffer Alloderm material and then, of the more elastic cellular component. Interestingly, vessels with the Alloderm material showed increased collagen content and encouraged collagen deposition by the cells as seen in the additional collagen lining the cells.

Additionally, cell nuclei were seen located in the fibrin gel and Alloderm, which indicates that the extracellular matrix encouraged cell migration and infiltration.

Inclusion of the Alloderm into the engineered rings significantly improved circumferential tensile mechanics compared to standard rings. This is due to the significant increase in the load-bearing collagen extracellular matrix protein provided by the Alloderm. These results are quite encouraging to progress towards clinical application, since the incorporation of the Alloderm elevated the engineered vessels' tensile strength to 1500 ± 334 kPa, which allows the engineered vessel to meet the comparative native adventitia tensile strength of 1430 ± 604 kPa[12]. The other important parameter for clinical application is the burst pressure. There was a significant difference in burst pressure with the addition of the Alloderm – however, the burst pressure needs further improvement in order to meet human blood pressure values. Our lab is currently testing methods to improve burst pressure in our vessels with promising preliminary results, which is the focus of an upcoming follow-up study. Nevertheless, the current burst pressure strength of 51.3 ± 2.19 mmHg of the Alloderm vessels is encouraging as it approaches human diastolic blood pressure values.

Interestingly, Alloderm rings exhibited a lower ultimate tensile strength and failure strength than Alloderm alone. This is due to the discrepancy in the cross-sectional area of each group that is inputted into the strength calculations. Stress is calculated as the force divided by the cross-sectional area. The rings have an inherent larger cross-sectional area due to the additional thickness as the cells and hydrogel pull the Alloderm into the ring shape. Alloderm alone remains at its original thickness. Thus, the thicker the tissue, the larger the cross-sectional area and thus the smaller the stress for a given force applied. This effect directly correlates to the parameter of strength which is determined from the stress-strain curve.

In the longitudinal direction, no significant differences were observed in forces associated with the elastic modulus and ultimate tensile strength between standard vessels and Alloderm rings, meaning that the addition of the Alloderm did not affect longitudinal vessel mechanics. Longitudinal strength of the engineered vessels with or with Alloderm could be improved. However, in vivo the vessels would not be subjected to major forces in that direction. Also, it has been shown that engineered vessels after implantation are remodeled with endogenous cell engraftment which further strengthens the tissue in all directions[2]. Regardless, the current study in our lab to improve burst pressure will concurrently strengthen the vessels in the longitudinal direction. Suture retention was not significantly different between standard engineered vessels and Alloderm vessels likely because suture retention relies on longitudinal structural components, similar to burst pressure strength. Hence, since burst pressure was not significantly different, it is not surprising that suture retention strength followed a similar trend.

Conclusions

Here, we demonstrate the incorporation of commercially available decellularized extracellular matrix Alloderm as a scaffold to significantly improves the mechanical properties of our engineered biological vascular grafts, a pre-requisite for meaningful clinical utility. Additionally, the added ECM advantageously

increased collagen content, improved ECM organization, increased mature collagen content, and encouraged cell engraftment. Our ongoing work on methods to improve burst pressure strength currently shows promising preliminary results, further increasing its relevance for prospective patient applications.

Declarations

Acknowledgements

We would like to thank Drs. Karin Przyklenk and Peter Whittaker for the helpful discussions. Allergan, plc (formerly LifeCell Corp.) provided the Alloderm material. BP was supported by the Wayne State University Thomas C. Rumble Fellowship. This work was in part supported by the Fisher Family Foundation grant administered through the Vascular Surgery Department at the Henry Ford Hospital.

Author Contributions

B.P. and M.T.L. designed the project. B.P., D.M.S. and A.R. performed the experiments. B.P., A.R., L.S.K., and M.T.L. interpreted the data. B.P. and M.T.L. wrote the main manuscript text and prepared all figures. All authors reviewed and edited the manuscript.

Competing Interests

The authors declare no competing interests.

References

1. Huang, A. H. *et al.* Biaxial Stretch Improves Elastic Fiber Maturation, Collagen Arrangement, and Mechanical Properties in Engineered Arteries. *Tissue Eng Part C Methods* **22**, 524–533 (2016).
2. Lawson, J. H. *et al.* Bioengineered human acellular vessels for dialysis access in patients with end-stage renal disease: two phase 2 single-arm trials. *Lancet* **387**, 2026–2034 (2016).
3. Goins, A., Ramaswamy, V., Lichlyter, D., Webb, A. & Allen, J. B. Fabrication of a bilayer scaffold for small diameter vascular applications. *J. Biomed. Mater. Res. Part A* **106**, 2850–2862 (2018).
4. Syedain, Z. H. *et al.* A completely biological 'off-the-shelf' arteriovenous graft that recellularizes in baboons. *Sci Transl Med* **9**, (2017).
5. Syedain, Z. H., Meier, L. A., Bjork, J. W., Lee, A. & Tranquillo, R. T. Implantable arterial grafts from human fibroblasts and fibrin using a multi-graft pulsed flow-stretch bioreactor with noninvasive strength monitoring. *Biomaterials* **32**, 714–722 (2011).
6. Syedain, Z. H., Meier, L. A., Lahti, M. T., Johnson, S. L. & Tranquillo, R. T. Implantation of completely biological engineered grafts following decellularization into the sheep femoral artery. *Tissue Eng Part A* **20**, 1726–1734 (2014).

7. Mehta, R. I., Mukherjee, A. K., Patterson, T. D. & Fishbein, M. C. Pathology of explanted polytetrafluoroethylene vascular grafts. *Cardiovasc. Pathol. Off. J. Soc. Cardiovasc. Pathol.* **20**, 213–221 (2011).
8. McAllister, T. N. *et al.* Effectiveness of haemodialysis access with an autologous tissue-engineered vascular graft: a multicentre cohort study. *Lancet* **373**, 1440–1446 (2009).
9. Wystrychowski, W. *et al.* First human use of an allogeneic tissue-engineered vascular graft for hemodialysis access. *J Vasc Surg* **60**, 1353–1357 (2014).
10. Nemeno-Guanzon, J. G. *et al.* Trends in Tissue Engineering for Blood Vessels. *J. Biomed. Biotechnol.* **2012**, 956345 (2012).
11. Sommer, G., Regitnig, P. & Holzapfel, G. A. Biomechanics of human carotid arteries: experimental testing and material modeling. *J. Biomech.* **39**, S325 (2006).
12. Holzapfel, G. A., Sommer, G., Gasser, C. T. & Regitnig, P. Determination of layer-specific mechanical properties of human coronary arteries with nonatherosclerotic intimal thickening and related constitutive modeling. *Am. J. Physiol. Heart Circ. Physiol.* **289**, H2048-58 (2005).
13. Zieman, S. J., Melenovsky, V. & Kass, D. A. Mechanisms, pathophysiology, and therapy of arterial stiffness. *Arter. Thromb Vasc Biol* **25**, 932–943 (2005).
14. Chen, H. & Kassab, G. S. Microstructure-based biomechanics of coronary arteries in health and disease. *J. Biomech.* **49**, 2548–2559 (2016).
15. Chen, H. *et al.* The layered structure of coronary adventitia under mechanical load. *Biophys. J.* **101**, 2555–2562 (2011).
16. Holzapfel, G. A., Gasser, T. C. & Ogden, R. W. A New Constitutive Framework for Arterial Wall Mechanics and a Comparative Study of Material Models. *J. Elast. Phys. Sci. solids* **61**, 1–48 (2000).
17. Lin, C.-J. *et al.* Heterogeneous Cellular Contributions to Elastic Laminae Formation in Arterial Wall Development. *Circ. Res.* **125**, 1006–1018 (2019).
18. Aziz, J. *et al.* Molecular Mechanisms of Stress-Responsive Changes in Collagen and Elastin Networks in Skin. *Skin Pharmacol. Physiol.* **29**, 190–203 (2016).
19. Halim, A. S., Khoo, T. L. & Mohd. Yussof, S. J. Biologic and synthetic skin substitutes: An overview. *Indian J. Plast. Surg.* **43**, S23–S28 (2010).
20. Nicoletti, G. *et al.* Versatile use of dermal substitutes: A retrospective survey of 127 consecutive cases. *Indian J. Plast. Surg.* **51**, 46–53 (2018).
21. Jansen, L. A., De Caigny, P., Guay, N. A., Lineaweaver, W. C. & Shokrollahi, K. The Evidence Base for the Acellular Dermal Matrix AlloDerm: A Systematic Review. *Ann. Plast. Surg.* **70**, (2013).
22. Wong, A. K. *et al.* Histologic analysis of angiogenesis and lymphangiogenesis in acellular human dermis. *Plast Reconstr Surg* **121**, 1144–1152 (2008).
23. Ye, K., Traianedes, K., Choong, P. F. M. & Myers, D. E. Chondrogenesis of Human Infrapatellar Fat Pad Stem Cells on Acellular Dermal Matrix. *Front. Surg.* **3**, 3 (2016).

24. Mangera, A., Bullock, A. J., Roman, S., Chapple, C. R. & MacNeil, S. Comparison of candidate scaffolds for tissue engineering for stress urinary incontinence and pelvic organ prolapse repair. *BJU Int* **112**, 674–685 (2013).
25. Yin, Z. *et al.* The effect of decellularized matrices on human tendon stem/progenitor cell differentiation and tendon repair. *Acta Biomater* **9**, 9317–9329 (2013).
26. Sandor, M., Singh, D., Silverman, R. P., Xu, H. & De Deyne, P. G. Comparative Host Response of 2 Human Acellular Dermal Matrices in a Primate Implant Model. *Eplasty* **14**, e7 (2014).
27. Ng, K. W., Khor, H. L. & Hutmacher, D. W. In vitro characterization of natural and synthetic dermal matrices cultured with human dermal fibroblasts. *Biomaterials* **25**, 2807–2818 (2004).
28. Pinnock, C. B., Meier, E. M., Joshi, N. N., Wu, B. & Lam, M. T. Customizable engineered blood vessels using 3D printed inserts. *Methods* **99**, 20–27 (2016).
29. Pinnock, C., Xu, Z. & Lam, M. Scaling of Engineered Vascular Grafts Using 3D Printed Guides and the Ring Stacking Method. *J. Vis. Exp.* **2017**, (2017).
30. Patel, B., Xu, Z., Pinnock, C. B., Kabbani, L. S. & Lam, M. T. Self-assembled Collagen-Fibrin Hydrogel Reinforces Tissue Engineered Adventitia Vessels Seeded with Human Fibroblasts. *Sci Rep* **8**, 3294 (2018).
31. Xu, H. *et al.* Host response to human acellular dermal matrix transplantation in a primate model of abdominal wall repair. *Tissue Eng. Part A* **14**, 2009–2019 (2008).

Figures

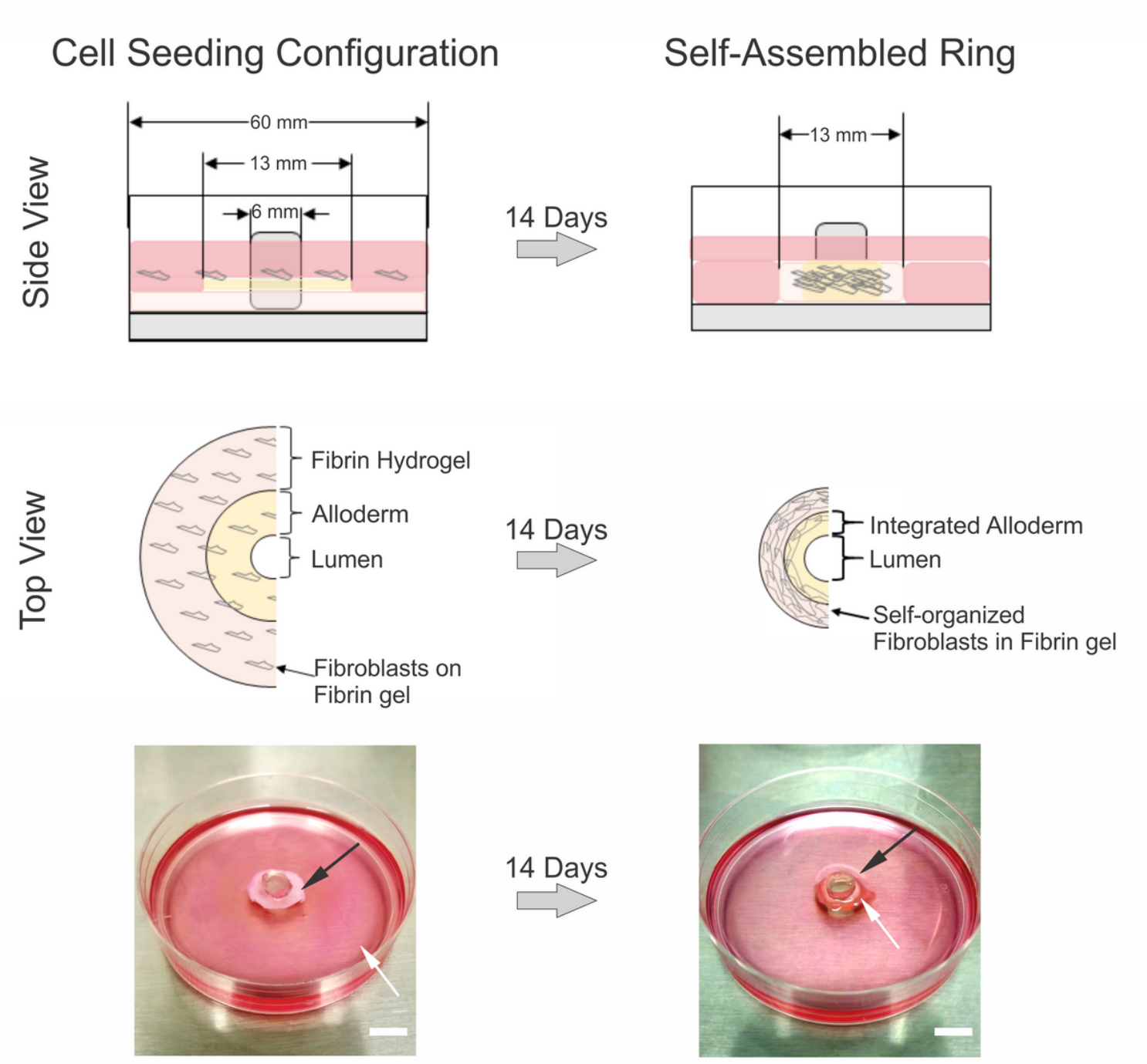

Figure 1

Diagram of self-assembled rings with incorporated Alloderm. Alloderm was integrated into the engineered vascular rings by placing the ECM material into the plate prior to cell seeding. Fibroblasts were seeded on top of the Alloderm and hydrogel, and the cells were able to infiltrate both the Alloderm ECM and hydrogel. Plate images show the progression of the engineered vascular ring formation 1 day and 14 days following seeding, showing the cell monolayer with hydrogel (edge indicated by white arrows) and the location of the Alloderm (black arrow) in the final ring tissue. Scale bar = 1 cm.

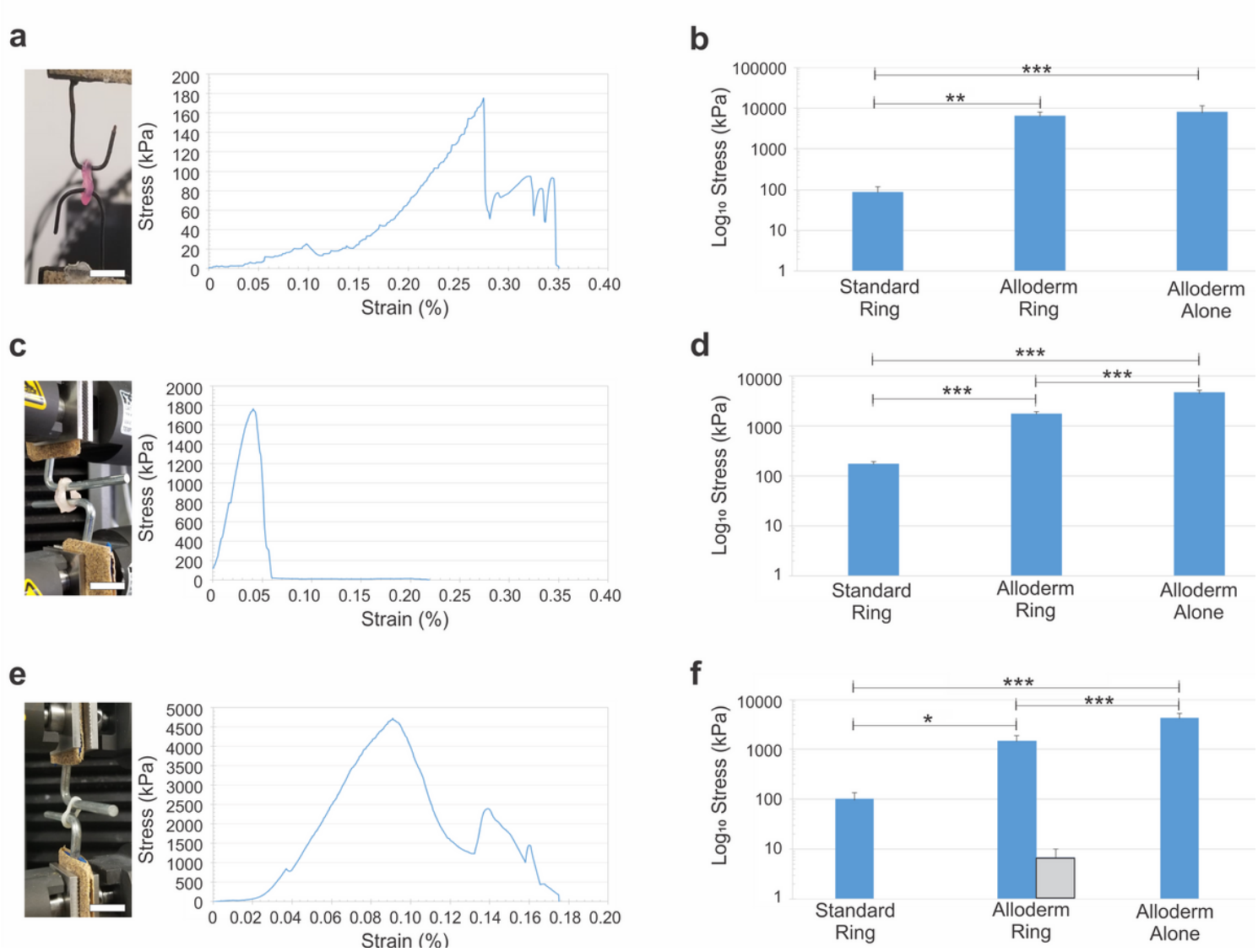

Figure 2

Significantly increased mechanical properties with inclusion of Alloderm into engineered vascular rings. (a,c,e) Average stress-strain curve of standard rings (n=5), Alloderm rings (n=5) and Alloderm alone (n=5). (b) Elastic modulus, (d) ultimate tensile strength and (f) failure strength shown for all groups. Elastic modulus, ultimate tensile strength and failure strength significantly improved with inclusion of Alloderm into the rings. Two failure strengths were exhibited by the Alloderm rings, indicating first rupture of the Alloderm (blue bar) and complete tissue failure of the rest of the ring composed of the cells and hydrogel (gray bar). Compared to Alloderm alone, Alloderm rings exhibited significantly lower elastic modulus, ultimate tensile strength, and failure strength. *p < 0.01; **p < 0.001; ***p<0.0001¬. Scale bar = 1 cm.

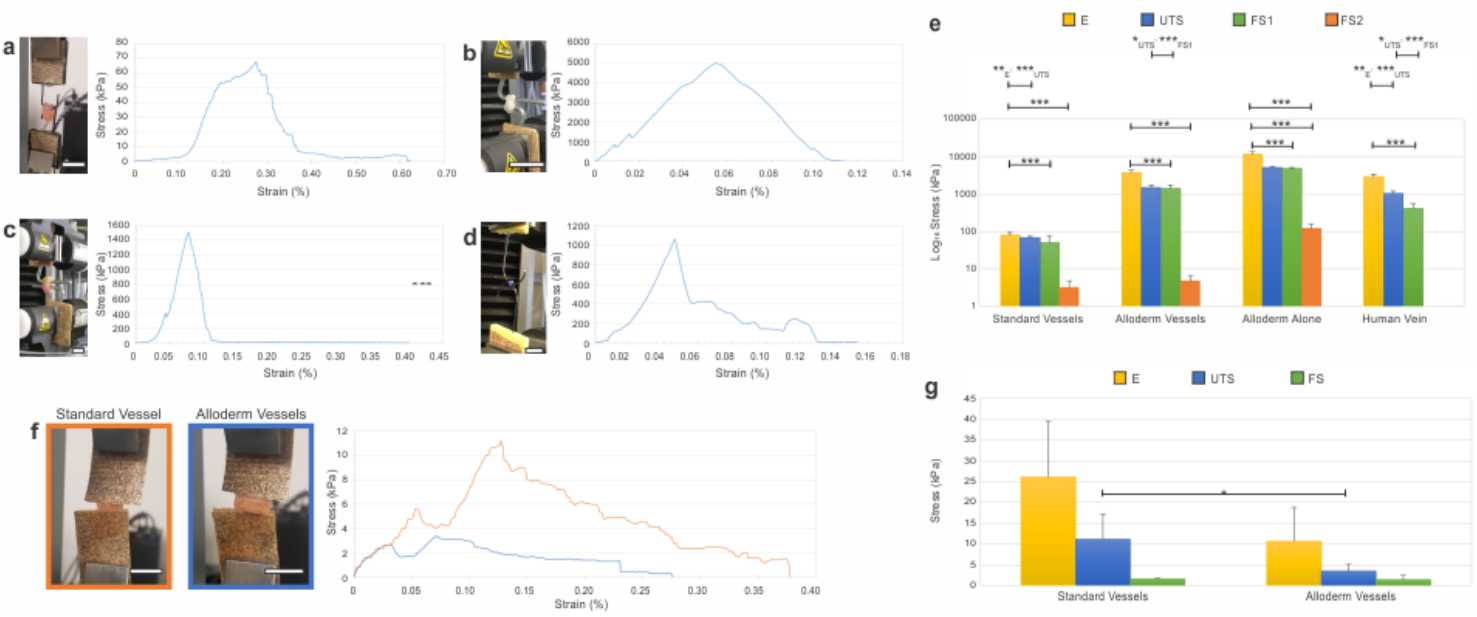

Figure 3

Significantly increased mechanical properties with inclusion of Alloderm into engineered vascular vessels. Average circumferential stress-strain curves for (a) standard vessels (n=5), (b) Alloderm alone (n=4), (c) Alloderm vessels (n=5), and (d) human diabetic saphenous veins (n=6). Average longitudinal stress-strain curves for (e) standard and alloderm vessels. Average circumferential elastic modulus (E), ultimate tensile strength (UTS), initial failure strength (FS1), and complete failure strength (FS2) for (f) standard and Alloderm vessels. Average longitudinal strengths for (g) standard and Alloderm vessels. Statistical significance between all moduli unless otherwise denoted. *p<0.05; **p<0.001; ***p<0.0001¬. Scale bar = 1 cm.

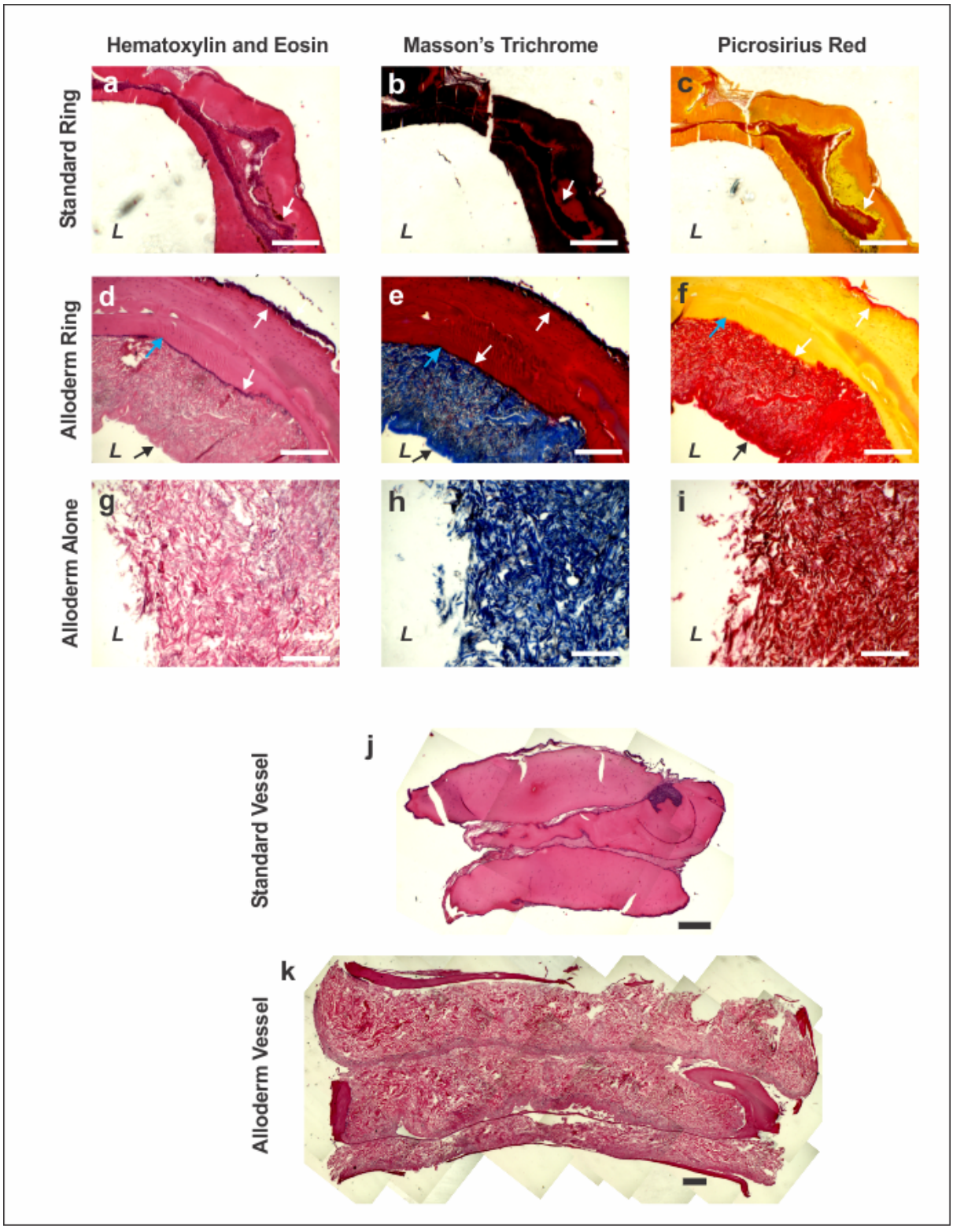

Figure 4

Extracellular matrix and cellular organization in engineered vascular rings and vessels improved with inclusion of Alloderm. H&E, trichrome and picrosirius red stains of (a,b,c) standard rings, (d,e,f) Alloderm rings and (g,h,i) Alloderm alone. Standard rings show an organization of cells (white arrow) surrounded by fibrin gel. The addition of Alloderm (black arrow) improved tissue organization by providing structural support for the cells (white arrows) and fibrin gel (blue arrow) around which to organize. Dense, organized

collagen is shown in the stains of Alloderm alone. Longitudinal sections of (j,k) H&E stained vessels show the ring-to-ring integration within the vessels, and the improvement of tissue organization with inclusion of Alloderm (k). L indicates lumen side. Scale bars = 200 μm.

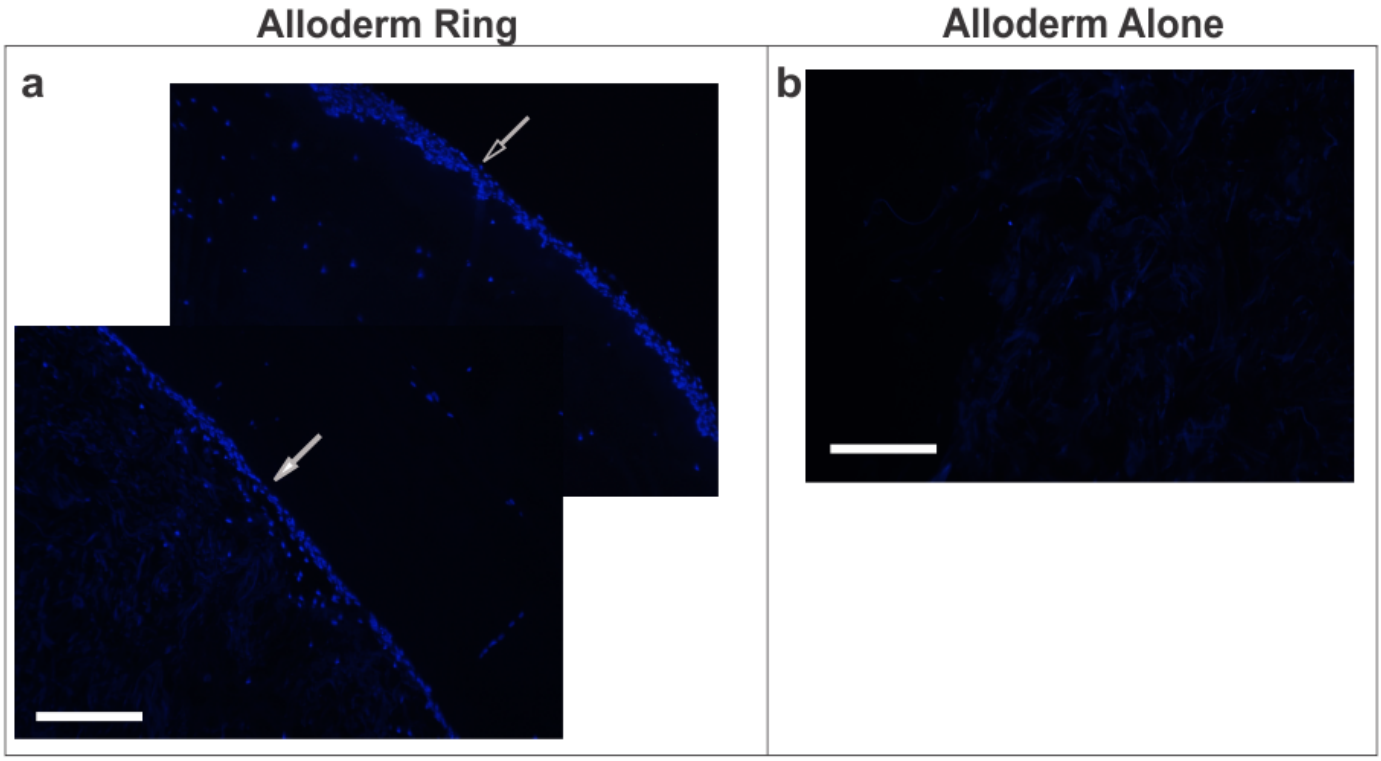

Figure 5

Cells infiltrated the Alloderm ECM in the engineered vascular tissue. DAPI stains of (a) an Alloderm-integrated vascular ring and (b) Alloderm alone. (a) Positive DAPI stain in Alloderm rings on the edge indicate cells seeded on the outer surface during the ring formation process (white open arrow), and positive DAPI stain in the Alloderm indicates cell infiltration (white closed arrow). (b) Lack of positive DAPI stain in the Alloderm alone verifies lack of cell presence prior to cell seeding, indicating that cells presence in the Alloderm in the rings (a) is due to cell infiltration. Scale bars = 200 μm.

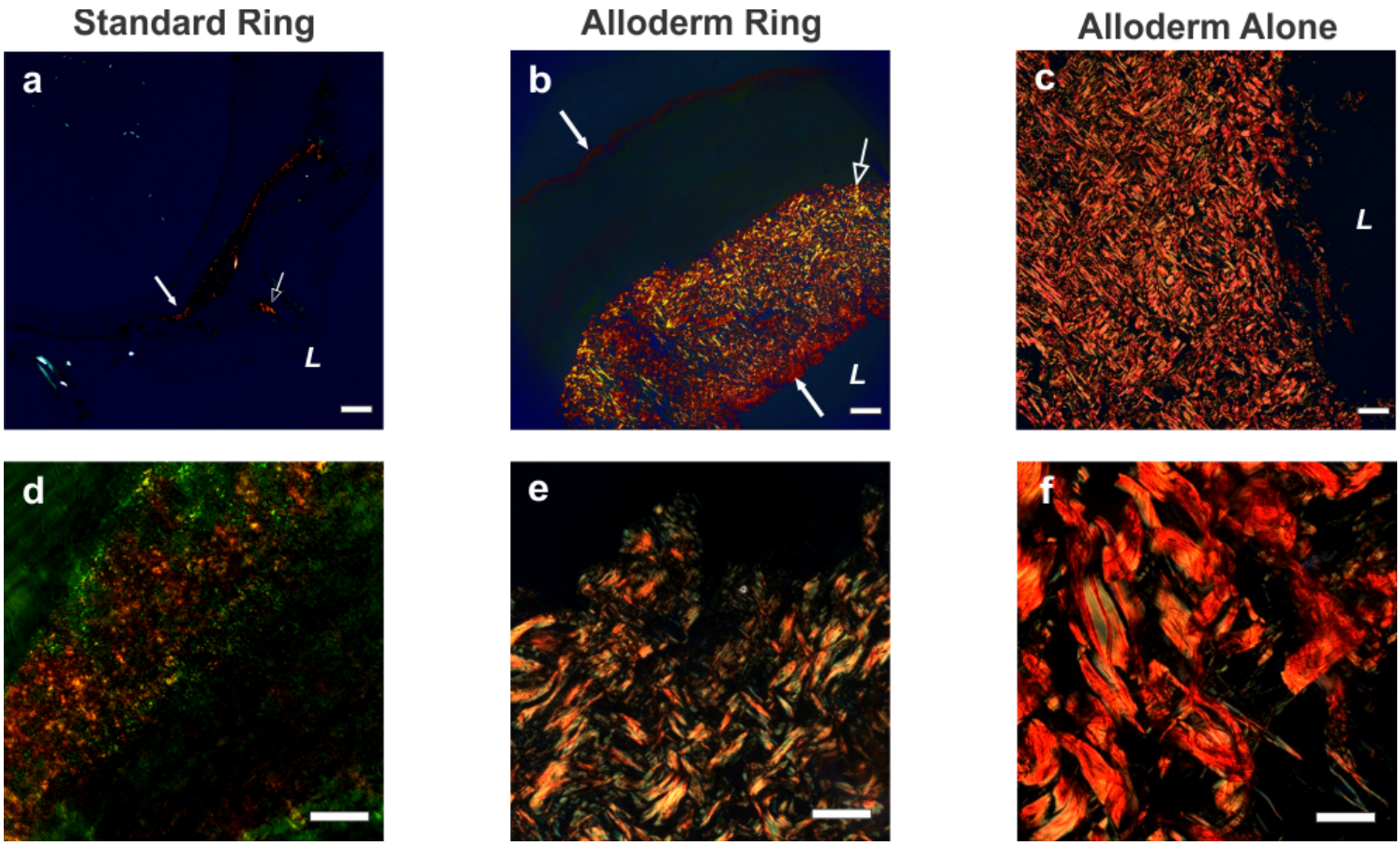

Figure 6

Increased collagen maturity of engineered vascular rings with incorporated Alloderm. Polarized light images of picrosirius red stained samples at (a-c) 5x magnification and (d-e) 40x magnification. Standard rings (a,d) exhibited mature red collagen fibers (white closed arrows) in the region of the cells and less mature yellow/orange fibers (white open arrows) in the fibrin gel. (b,e) Alloderm-integrated rings exhibited a mix of mature red collagen fibers and less mature yellow/orange fibers, along with green fibers indicating least maturity which was likely newly deposited by the cells. More mature red collagen fibers were present in the (c,f) Alloderm group, with very few green fibers. (a-c) scale bars = 200 μm; (d-f) scale bars = 100 μm; L indicates the lumen side.

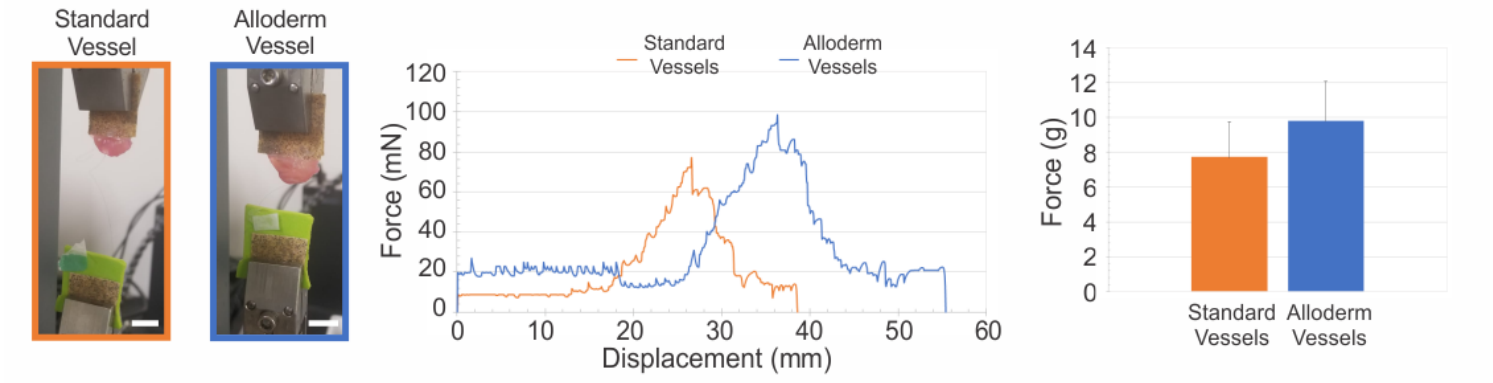

Figure 7

Average suture retention strength of engineered vessels increased with inclusion of Alloderm. Suture retention testing was performed on standard vessels (n=5) and Alloderm vessels (n=5). One end of the vessel was fixed to the tensile testing machine with sandpaper, with the suture glued to the other hook as shown. Both vessels experienced similar force output trends with respect to displacement. Alloderm vessels had a higher average maximum force compared to standard vessels. Scale bar = 1 cm.

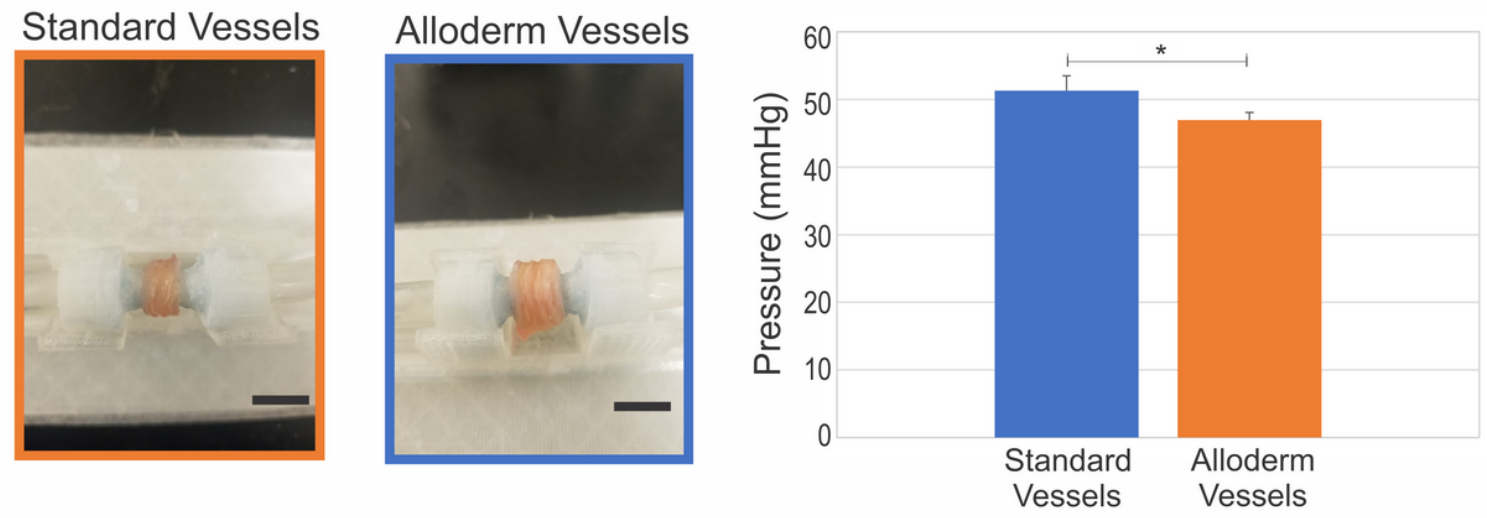

Figure 8

Burst pressure testing of engineered vessels. Standard vessels without (n=5) and with Alloderm (n=5) were placed under increasing pulsatile flow until failure. Vessels are shown loaded into the custom perfusion system used to perform the burst pressure tests. Alloderm vessels had significantly higher burst pressure compared to vessels without Alloderm (*$p<0.005$). Scale bars = 1 cm.

Supplementary Files

This is a list of supplementary files associated with this preprint. Click to download.

- SupFigure1.tif
- SupplementalTables.docx
- SupplementalVideo1.mov